High Temperature Corrosion of Materials
https://doi.org/10.1007/s11085-024-10281-8

ORIGINAL PAPER

Understanding the Phenomenon of High Temperature Hydrogen Attack (HTHA) Responsible for Ferrito-Pearlitic Steels Damage

N. Chevreux[1] · C. Flament[1] · O. Gillia[1] · T. David[1] · R. Goti[2] · C. Le Nevé[2] · E. Andrieu[3]

Received: 17 July 2024 / Revised: 17 July 2024 / Accepted: 21 July 2024

Abstract
This article focuses on the fine characterization of steels commonly used in the petrochemical industry damaged by the phenomenon of high temperature hydrogen attack (HTHA). The study was conducted in two steps. To begin with, a damaged 0.5-Mo pearlitic steel from the petroleum refineries, submitted to HTHA for decades, was characterized in detail using multiscale electron microscopy techniques. As part of an upstream study to better understand the onset and the growth of cavities, a brand new SA516 grade 60 low carbon–manganese steel was subsequently exposed to accelerated HTHA conditions through interrupted cycles carried out in autoclaves and then examined. Numerous cavities, plausibly filled with methane, were noticed in both materials. These cavities were mostly located at ferrite–pearlite grain boundaries along carbides and at triple grain boundaries near large carbides. The 0.5-Mo pearlitic steel showed cavities reaching significant sizes, up to 1 µm, but surprisingly no cracks were observed in the depth of the pipe. The major outcome is that 3D focused ion beam–scanning electron microscopy combined with transmission electron microscopy (TEM) analyses unveiled different natures of precipitates as well as in and nearby HTHA cavities for both 0.5-Mo and low carbon–manganese steels. Inclusions, likely AlN, but also Mo- and Cu-rich precipitates were observed in cavities of the industrial steel. These results confirmed a previous study performed on a similar industrial steel that drew a possible correlation between cavities nucleation and the intersection of transgranular inclusion-enriched plane with a grain boundary or carbides in pearlite grains (Flament in Microscopy and Microanalysis 28:1602–1604, 2022).

Keywords HTHA · Hydrogen · Low carbon steels · Pressure vessels

Extended author information available on the last page of the article

Published online: 08 August 2024

Introduction

High Temperature Hydrogen Attack (HTHA) affects low carbon ferrito-pearlitic steels submitted to hydrogen involving hydrogen pressures higher than 3.5 bar (50 Psi) and temperatures above 204 °C (400 °F) [2]. Those steels are used for manufacturing pressure vessels and piping. Oil and gas industrial equipment is damaged by this phenomenon, yet, and it is likely to occur in the development of promising technologies close to the carbon neutrality such as the power to gas and biomass retreatments [2–4]. Symptoms of this attack are concurrently surface decarburization [2, 5] and creation of methane-filled cavities (whose pressure can reach thousands of bars) in depth of the material [6] [7]. Hydrogen reacts with the free carbon in solid solution and at grain boundaries. This source of carbon is limited and quickly drawn off. Carbon from carbides is then consumed [8] to form methane according to the general equation:

$$M_xC_y + 4yH \rightarrow xM + yCH_{4(gas)} \quad (1)$$

As methane molecules are too large to diffuse in the steel, the methane pressure in cavities builds up becoming the driving force for their growth [2, 5, 6]. Thus, as aging in hydrogen atmosphere progresses, the cavities expand and coalesce until cracks open. The mechanical strength of the damaged steels is thus irreversibly reduced [9]. This can lead to rupture in the most serious cases [10]. It is possible to predict if a steel grade used in piping is prone to exhibit degradations due to HTHA by using the Nelson's diagram showing the service temperature as function of the H_2 partial pressure. These curves are published by the American Petroleum Institute (API) and are drawn based on feedbacks from petroleum facilities whose materials were assessed as "satisfactory" or showing failures. These empirical curves are regularly updated. As described by Cantwell [4], the 0.5-Mo steel curve is among those that have changed the most over the years due to multiple failures that occurred in the safe operating area. Eventually, the 0.5Mo steel Nelson's curve got removed of the API 941 in 1990 and the PWHT-carbon steel curve was designated as their reference [2]. Post-Weld Heat treatment (PWHT) is a stress-relieving thermal treatment, performed below critical transformation temperatures of a material to reduce its residual stresses.

Although this phenomenon is widely known, both onset and growth of cavities remain not well understood. The aim of this study is to emphasize potential correlations between the microstructure of the steel and the initiation of HTHA cavities as well as the aggravation of HTHA-induced degradations. To this end, a degraded 0.5-Mo pearlitic steel from the petroleum industry whose pressure vessels and pipes were submitted to HTHA conditions for decades has been thoroughly characterized. Scanning and transmission electron microscopy (SEM, TEM) as well as 3D focused ion beam–SEM techniques was carried out. To investigate the nucleation and growth kinetics of cavities, very first stages of the attack were studied through a complementary experimental program. This program involves subjecting a brand new SA516 gr 60 low carbon–manganese steel to accelerated HTHA conditions through interrupted cycles in autoclaves followed by characterization.

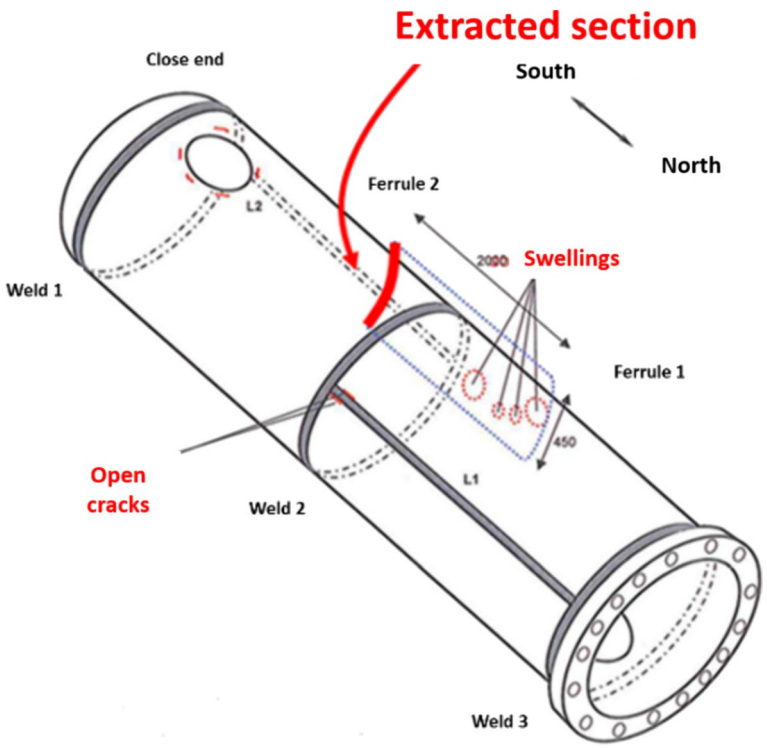

Fig. 1 0.5-Mo steel extracted section from a fluid heat exchanger

Table 1 Composition in wt.% of the 0.5Mo low carbon steel

C	S	N	O	Mn	Mo	Cr	V	P	Si	Ni	Al	Cu
0.17	0.017	0.008	< 0.005	0.73	0.62	0.092	< 0.005	0.014	0.28	0.21	0.031	0.38

Experimental Procedures

5-Mo Pearlitic Steel

The 0.5-Mo pearlitic steel section characterized in this study was extracted from a 27-mm-thick fluid heat exchanger (as shown in Fig. 1) with a diameter of 750 mm. This exchanger was submitted to a temperature of 400 °C at an internal pressure of 20 bars with a H_2 partial pressure of 18 bars for a 37-year period. It contained both oil and H_2.

The initial microstructure of the steel is unknown. The microstructure was characterized as it is after 37 years of service. Table 1 presents the composition of the steel as measured by elementary analysis for C, N, O, S elements and by inductively coupled plasma–atomic emission spectroscopy (ICP-AES) for the other elements.

SA516 Steel Low Carbon–Manganese Steel

As PWHT-carbon steels and 0.5Mo steels are described by the same Nelson's curve, a SA516 low carbon–manganese steel was selected to endure accelerated aging under a H_2 rich atmosphere. The material was obtained by continuous casting carried out in arc furnace. Table 2 presents the chemical composition of the casted steel given by the supplier:

The casted 225-mm-thick plate is then hot-rolled to achieve a final plate thickness of 27 mm. The plate was finally heat-treated at 600 °C for 1 h in order to simulate a PWHT-type stress-relieving treatment. H_2 aging was performed in autoclaves. Two series under 69 bars of H_2 (1000 psi) were simultaneously achieved: one at 304 °C and the other at 400 °C. Aged samples were extracted every 300 h to be characterized by SEM techniques. Currently, 5 cycles at 304 °C have been completed for the first batch of samples and 1 cycle at 327 °C followed by 4 cycles at 400 °C has been performed for the second batch of samples.

Characterization Techniques

In order to characterize the microstructure of the degraded steels, samples were first finely polished with colloidal silica and then observed using a Zeiss Merlin field emission gun scanning electron microscope (FEG SEM) featuring two X-rays energy dispersive spectroscopy (EDX) detectors from Bruker controlled by Esprit Software. SEM provides a direct view of various zones showing HTHA-induced cavities but restricts to a 2D perspective. In the framework of a multiscale characterization as well as to exhibit a possible link between the steel microstructure and HTHA cavities, a Zeiss CB 550 focused ion beam–scanning electron microscope (FIB-SEM) was used to achieve a 3D characterization. Atlas software allowed to perform automatic acquisitions of secondary electron image slices. A slicing step of 3 nm was chosen in order to finely observe cavities and distinguish inclusions; the voxels size is thus 9 nm^3. Both Python scripts and ImageJ software were used to perform the alignment and process of the slices. The obtained stack is subsequently segmented thanks to Ilastik software. Dimensions of the final generated volume are $9 \times 5.5 \times 5.5$ μm^3. A Zeiss 550 CB FIB was used to lift out a TEM lamella from the samples previously prepared for SEM observations in an analogous zone to the one studied by slice and view. Finally, scanning (S)TEM-HAADF (High Angle Annular Dark Field) characterizations were carried out in a Thermofischer Tecnai Osiris FEG TEM operating at 200 kV combined with a Super-X system featuring 4 silicon drift detectors for EDX analyses.

Table 2 Composition in wt.% of the SA516 gr60 low carbon steel

C	S	N	O	Mn	Mo	Cr	V	P	Si	Ni	Al	Cu
0.18	< 0.001	–	–	1.242	0.003	0.066	0.002	0.007	0.39	0.03	0.028	0.034

Results

5-Mo Pearlitic Steel

Samples from both the inner and the outer part of the pipe were examined by SEM. Carbides appear white and ferrite gray in Fig. 2a–d. Cavities, corresponding to the black spots pointed out in Fig. 2a–d, are mostly located at ferrite–pearlite grain boundaries and along carbides. Cavities are noticed both in the inner and outer parts of the exchanger. Still, in the outer part cavities are less numerous than in the inner part, see Fig. 2a and b. These cavities display diameters from few hundred nanometers up to 1 µm. No cracks in the depth of the material are observed. It seems that the attack is extremely heterogeneous as some grain boundaries of pearlite grains are completely cavities-free while few microns away other pearlite grain boundaries are presenting a profusion of cavities. The steel presents a ferrito-pearlitic microstructure. However, as shown in Fig. 2c–d no lath-like but globularized cementite carbides are noticed at grain boundaries. The morphology of carbides in the inner as well as the outer specimens might be related to the phenomenon of temper aging.

The industrial steel has been finely characterized thanks to the 3D FIB-SEM slice and view technique. Figure 3a-l shows 2D SEM successive slices taken after some steps of the ion abrasion in a zone unveiling two cavities. Cavities noticed at grain boundaries appear dark black on these images. These cavities are located in a triple grain boundary and are very faceted, which could be due to a growth following

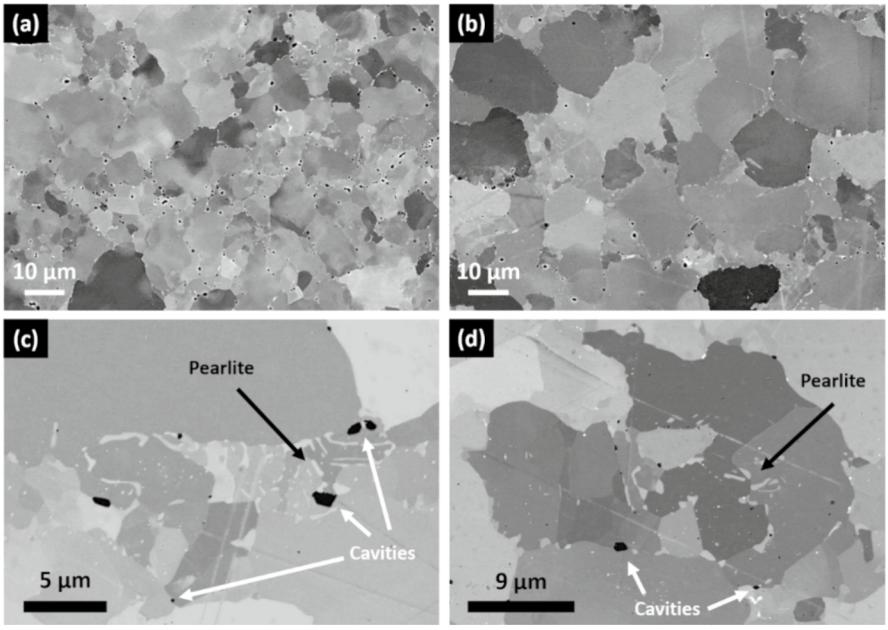

Fig. 2 SEM observations of the 0.5Mo steel after HTHA. Large-scale views of (**a**) the inner part and (**b**) the outer part of the fluid heat exchanger. Small-scale views of typical pearlitic grains morphology (**c**) in the inner part and (**d**) in the outer part of the exchanger

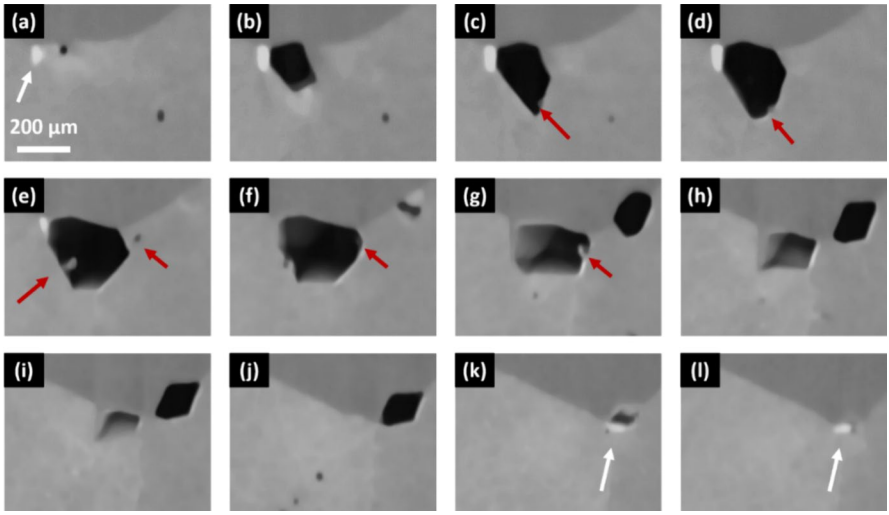

Fig. 3 2D SEM images showing the link between different types of inclusions and cavity nucleation at grain boundaries

the closed packed plans of ferrite crystal structure. As long as the ion abrasion progresses, two different precipitate contrasts were exhibited as shown in Fig. 3 (i.e.) a white and bright one (white arrows) touching the edge of cavity and a dark gray one (red arrows) located in the cavity. Such a link between inclusions of AlN type and cavities has already been highlighted [1]. As their nature could not be determined by 3D FIB-SEM, TEM analysis was conducted in order to get complementary information about these different inclusions.

STEM-EDX maps were taken in two different zones. The first EDX map presented in Fig. 4.a was obtained in a cementite-attacked zone. It appears that the cementite is not only composed of Fe but also Mn, traces of Cr are also observed. The chemical analysis of the identified cavity exposes that there is no AlN inclusion in it. However, co-segregation of Mo and Si is observed. The carbon map gives the impression that this Mo inclusion contains carbon. Furthermore, Cu precipitates appear as well as in and around HTHA cavities. Small Cu-rich precipitates are noted at grain boundaries and in dislocations. A 70-nm curvy and elongated Cu precipitate seems to be present in the cavity. The second zone examined was taken in a completely cavity-free ferrite grain, as shown in Fig. 4b. EDX mapping shows first a rod like AlN inclusion where Si, Cu, and Mo segregated along. A second precipitate rich in Mo and C appears. It is assumed to be Mo_2C carbides. Cu segregated around this Mo-rich precipitate. Finally, a 50-nm-long inclusion rich in Cu is present in the ferrite matrix.

SA516 steel low carbon–manganese steel.

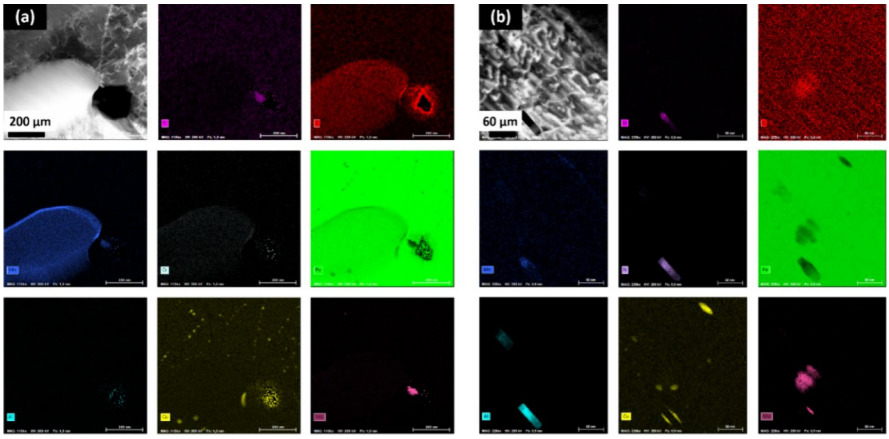

Fig. 4 STEM-HAADF and EDX maps (**a**) of a cavity containing a Mo-rich inclusion. **b** Different precipitates in a cavity-free ferrite grain

SEM observations of the SA516 steel reveal that the brand new material exhibits a typical ferrito-pearlitic microstructure. $(Fe,Mn)_3C$ type carbides were confirmed by TEM (not shown in this article). To begin with, for a same H_2 partial pressure of 69 bars and for a same number of cycles it appears that specimens aged at 400 °C display a greater number of cavities compared to those aged at 304 °C which has none, as shown in Fig. 5a and Fig. 5b. As anticipated, most attacked samples exhibit cavities mostly at ferrite–pearlite grain boundaries along carbides as well as triple grain boundaries, especially nearby large carbides.

Furthermore, it emerges in 400 °C-aged specimens that presumed HTHA cavities are located at the junction of carbides at grain boundaries with an alignment of small inclusions, see Fig. 6a–d. SEM–EDX analysis identified them as AlN inclusions.

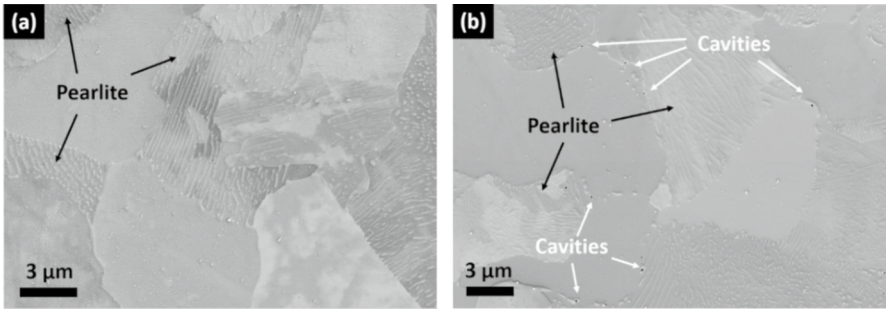

Fig. 5 SEM–secondary electrons images of the SA516 steel aged under PH2 = 69 bars. **a** After 5 cycles of 300 h at 304 °C. **b** After a first cycle of 300 h at 327 °C followed by 4 cycles of 300 h at 400 °C

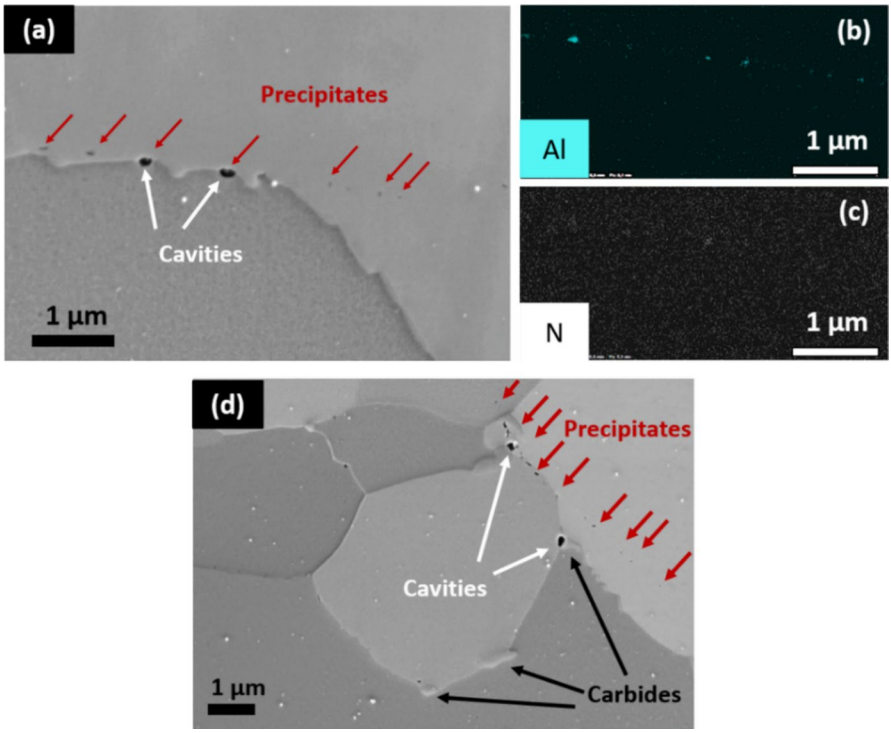

Fig. 6 SEM images of the SA516 steel aged under PH2 = 69 bars: **a** 300 h at 327 °C then 300 h at 400 °C (1000 psi). **b**,**c** Al and N SEM–EDX maps suggesting AlN precipitates in voids. **d** 300 h at 327 °C followed by 4cycles of 300 h at 400 °C

Discussion

Mo Pearlitic Steel

Multiscale electron microscopy examinations of the 0.5 Mo pearlitic steel (SEM, 3D FIB-SEM and TEM complementary analyses) exhibited the presence of various inclusions at the edges of cavities. Each cavity studied by TEM presents an inclusion. The absence of AlN in the TEM–EDX analyzed cavity could be explained either by the fact that it got removed during the lamella preparation or might imply that not only AlN precipitates are assisting the onset of cavities. Indeed, it is possible that Cu or Mo_2C precipitates have the same effect as AlN on the nucleation of HTHA cavities. 0.5 Mo steels are widely used in industrial applications (piping, pressure vessels, and heat exchangers) due to their good creep resistance. Indeed, addition of Mo enhances the creep resistance of steels and promotes the formation of stable carbides as MC, M_2C ξ-M_3C, M_6C, or stoichiometry [11–13]. However, under high temperature service conditions pipes made with these steels can still exhibit creep. Several studies highlighted the synergy between creep and HTHA [14–17]. R.E Allen and al. [14] even stated that

the rate of hydrogen attack was dramatically accelerated by creep. Myers and al. [18] have studied the intergranular creep damage and noticed that M_3C and M_2C carbides are enabling the nucleation of creep cavities. Formation of creep cavities near Mo_2C and Fe_3C concurrently to the hydrogen exposure may dramatically aggravate HTHA damages and might explain why large cavities are observed in the material.

Although the cavities observed by SEM display significant sizes, no cracks have been observed. Moreover, due to temper aging the steel does not present a typical ferrite–pearlitic microstructure as no lath-like but globular cementite carbides are observed [19]. Due to a 37-year exposure period to a temperature of 400 °C, spheroidization of cementite occurs and very stable round-shaped carbides are formed along grain boundaries. Thus, ferrite/cementite surface energy and interfacial area per unit of volume decrease. According to Weiner [20], spheroidized carbides appear to be more resistant to HTHA. As hydrogen has a smaller surface to interact with carbides, it would induce much localized interactions and so limiting the coalescence of cavities. Therefore, the formation of cracks might be hindered.

SA516 Steel Low Carbon–Manganese Steel

Specimens aged at 400 °C under a H_2 partial pressure of 69 bars unveil that very first cavities nucleate preferentially at perlite–ferrite interfaces and at triple grain boundaries along large carbides. In pure pearlitic areas, hydrogen might be too diluted to lead to a preferentially attacked zone as it has access to a massive but a very scattered amount of carbon. 304 °C-aged samples show very few cavities compared to the 400 °C-aged ones for a given number of aging cycles. The explanation is not so trivial considering that theoretically the methane pressure is decreasing with an increase in temperature [6]. The mechanical strength is also decreasing with an increase in temperature. In this decrease competition, the apparition of more cavities at higher temperature suggests that the strength loss becomes predominant. Nevertheless, the increased cavitation tendency may be due to other mechanisms such as enhanced diffusion coefficient of hydrogen in steels with temperature [21]. Such observations could result from the fact that the temperature induces more vacancies at higher temperatures and thus might facilitate the onset of cavities [22].

Additionally, SA516 aged steels display cavity nucleation along AlN plans, which tends to confirm the initiating role of precipitates. These observations are similar to what has been seen in a previously studied 0.5-Mo pearlitic steel in which numerous cavities were identified at the intersection of AlN inclusions enriched planes and pearlite grains [1]. Thus, AlN inclusions distributed in former austenitic grains boundaries [23, 24] seem to be initiators of HTHA cavities. AlN–matrix interface may trap elements such as Cr, Cu, and Mo much larger than H. Thus, hydrogen could be trapped at such interface nearby a carbide, having access to a significant amount of carbon to form CH_4. To enable the formation of CH_4 molecules, a certain available space is required. Vacancies clusters that might be present at the AlN–matrix interface may allow the formation of early cavities filled with CH_4 and then coupled with the high internal CH_4 pressure be a driving force behind their

growth. To better comprehend phenomena occurring at the matrix–AlN interfaces, fine-scale complementary studies will be conducted by high-resolution transmission electron microscopy. According to the initial microstructure, it seems unlikely that precipitation is the only factor explaining the high heterogeneity of the attack. Localized residual stresses in samples and the presence of deformation inhomogeneities might have a significant impact on the nucleation of cavities. As a result, electron backscatter diffraction (EBSD) analyses will be performed both in slightly and highly attacked zones to analyze grain misorientations and investigate possible local visco-plasticity in neighboring grains.

Conclusion

HTHA cavities were detected by electron microscopy techniques in a 0.5-Mo pearlitic steel from the petroleum refineries subjected to HTHA for decades but also were initiated in a low carbon–manganese steel submitted to accelerated HTHA conditions through interrupted cycles. Each sample displays a very high heterogeneity of attack. Samples exhibit attack morphologies that are substantially similar across various damaged zones. Indeed, cavities were noticed mostly at ferrite–pearlite grain boundaries along carbides and at triple grain boundaries near large carbides. Furthermore, precipitates seem to have a significant initiating role in the nucleation of HTHA cavities. These observations are in line with the literature [25]. In the recent SA516 steel, AlN precipitates appear to be highly correlated with the apparition of cavities. Although no AlN precipitates were directly identified in the 0.5-Mo pearlitic steel, Mo- and Cu-rich precipitates were highlighted in conjunction with cavities. Observations in the SA516 steel correlates with what has already been seen in a previous study in a 0.5-Mo steel from the industry [1]. Still, deeper investigations and fine characterizations of the AlN–matrix interface through high-resolution transmission electron microscopy appear to be mandatory to better comprehend the initiation and growth of methane cavities.

Acknowledgements This study was a collaborative effort between CEA and TotalEnergies. Electron microscopy analyses were achieved at the CEA NanoCharacterization Platform (PFNC)-Minatec, supported by the “Recherche Technologique de Base” and "France 2030-ANR-22-PEEL-0014" programs of the French National Research Agency (ANR). The authors express their gratitude to Bastien Chareyre and Sylvain Pillot for providing and conducting the accelerated aging in autoclaves in Industeel-Arcelor-Mittal facilities. The authors gratefully acknowledge Nathalie Ladrat for TEM sample preparation.

Author Contribution N.C, C.F, O.G, and T.D investigated, performed the experiments, and analyzed the data. N.C, C.F, O.G wrote the original draft. C.F, O.G, R.G, C.L, and E.A supervised the research work. R.G and C.L acquired the funding. R.G managed the project administration. All authors reviewed the manuscript and agreed to be held accountable for the work.

Funding Open access funding provided by Commissariat à l’Énergie Atomique et aux Énergies Alternatives.

Data Availability No datasets were generated or analyzed during the current study.

Declarations

Conflict of interest The authors declare that they have no known competing financial interests or personal relationships that could have appeared to influence the work reported in this paper.

References

1. C. Flament, et al., *Microscopy and Microanalysis* **28**, 2022 (1602). https://doi.org/10.1017/S1431927622006419.
2. *API Recommended Practice 941*, 8th ed. 2016.
3. G.A. Nelson, *Proceedings API M* (1949).
4. J.E Cantwell, *Journal of Materials Engineering and Performance*, 58 (1994).
5. E. E. Fletcher and A. R. Elsea, *Materials Science, Engineering*, (1964).
6. G. R. Odette and S. S. Vagarali, *Metallurgical Transactions A*. **13**, 1982 (299).
7. M. Mckimpson and P. G. Shewmon, *Metallurgical Transactions A* **12**, 1981 (825).
8. R.E. Allen, R.J. Jansen, P.C. Rosenthal, and F.H. Vitovec, *American Petroleum Institute—Proceedings* 42, 452 (1962).
9. R.E. Allen, R.J. Jansen, P.C. Rosenthal, and F.H. Vitovec, *American Petroleum Institute—Proceedings*, (1961).
10. CATASTROPHIC RUPTURE OF HEAT EXCHANGER (SEVEN FATALITIES)-TESORO ANACORTES REFINERY, U.S. CHEMICAL SAFETY AND HAZARD INVESTIGATION BOARD, 2010–08-I-WA, mai 2014.
11. K. Kuo, *The Journal of the Iron and Steel Institute* **173**, 1953 (363).
12. K. Kuo, *Acta Metallurgica* **1**, 1953 (301).
13. K. M. Reddy, T. N. Rao, J. Revathi, and J. Joardar, *Journal of Alloys and Compounds* **494**, 2010 (86).
14. R. Allen, P. Rosenthal, F. Vitovec, *American Petroleum Institute—Proceedings*, 1962
15. J. Coombs, R. Allen, F. Vitovec, *American Petroleum Institute—Proceedings*, 1965.
16. K. Yokogawa, S. Fukuyama, K. Kudo, and P. G. Shewmon, *International Journal of Pressure Vessels and Piping*. **37**, 1989 (365).
17. L. Looney, R. C. Hurst, and D. Taylor, *Journal of Materials Processing Technology* **77**, 1998 (25).
18. M. R. Myers, R. Pilkington, and N. G. Needham, *Materials Science and Engineering* **95**, 1987 (81).
19. S. Brett *et al.*, Materials Science 6, (2005).
20. L. C. Weiner, *Corrosion* **17**, 1961 (137t).
21. J. Chêne, *Plastics and the Environment* **2007**, 2009 (131–145).
22. H. Mehrer, *Diffusion in Solids: Fundamentals, Methods, Materials, Diffusion-Controlled Processes*. in Springer Series in Solid-State Sciences. Springer Berlin Heidelberg, 2007. [En ligne]. Disponible sur: https://books.google.fr/books?id=IUZVffQLFKQC
23. F. G. Wilson and T. Gladman, *International Materials Review* 33 (1988).
24. R. Radis and E. Kozeschnik, *Materials Science Forum* **636–637**, 2010 (605).
25. M. L. Martin, M. Dadfarnia, S. Orwig, D. Moore, and P. Sofronis, *Acta Materialia* **140**, 2017 (300).

Authors and Affiliations

N. Chevreux[1] · C. Flament[1] · O. Gillia[1] · T. David[1] · R. Goti[2] · C. Le Nevé[2] · E. Andrieu[3]

✉ C. Flament
camille.flament@cea.fr

[1] Université Grenoble Alpes, CEA-LITEN, Grenoble, France

[2] Total Research and Technology Gonfreville, TotalEnergies, Harfleur, France

[3] CIRIMAT-ENSIACET, 31030 Toulouse, France